electronics

MDPI

Article

Biochar-Coated Drywall Panels for Electromagnetic Shielding Applications in the K-Band

Giuseppe Ruscica [1,*], Patrizia Savi [2], Michele Perotti [2] and Isabella Natali Sora [1]

1 Department of Engineering and Applied Sciences, Università di Bergamo, 24044 Dalmine, Italy; isabella.natali-sora@unibg.it
2 Department of Electronics and Telecommunications, Politecnico di Torino, 10129 Turin, Italy; patrizia.savi@polito.it (P.S.); michele.perotti@polito.it (M.P.)
* Correspondence: giuseppe.ruscica@unibg.it

Abstract

With the rise of telecommunication systems in recent decades, the implications for human health have prompted a search for ways to reduce the impact of electromagnetic waves in buildings when necessary. A viable and promising solution to realize electromagnetic shielding could be the use of drywall panels coated with a biochar paste, as proposed in this study. Biochar (bio-charcoal), a low-cost and carbon-based material, can be obtained by the thermochemical conversion of different biomass sources. A commercial wood-based biochar thermally treated at 750 °C is considered in this work. Transmission coefficients of several gypsum board elements with a biochar coating are measured in the frequency K-band (18–27 GHz). In addition, the SE of a double panel configuration, obtained by joining two coated boards to form a multilayer structure, is evaluated. The results show that the biochar coating significantly enhances the SE compared to uncoated drywall. At the highest biochar loading investigated (0.20 g/cm^2), the shielding effectiveness consistently exceeds 27 dB for single panels and 46 dB for double panels across the entire frequency band. These findings indicate that biochar-coated drywall systems offer a practical and sustainable solution for integrating electromagnetic shielding into building envelopes, paving the way for innovative applications in indoor exposure control.

Keywords: shielding effectiveness; electromagnetic shielding; biochar; sustainable building materials; drywall; gypsum board; K-band; indoor exposure control

1. Introduction

Electromagnetic radiation in the microwave and millimetre-wave range is increasingly pervasive in modern environments due to the widespread use of satellite links, wireless communication systems, and emerging high-frequency services. Beyond unintentional environmental exposure, intentional electromagnetic interference (IEMI)—i.e., the deliberate injection of conducted or radiated electromagnetic energy to disturb or damage electronic systems—has become a relevant concern for critical infrastructures and power-electronic equipment, motivating systematic susceptibility assessment, simulation and mitigation strategies [1,2]. Besides thermal absorption by polar molecules, several studies have reported biological responses that cannot be explained solely by heating effects, including alterations in microorganisms exposed to microwaves [3] and possible effects of radiofrequency electromagnetic-field exposure on the human central nervous system [4]. A practical strategy to mitigate indoor exposure is to integrate shielding materials into the

Academic Editor: Jianguo Zhu

Received: 25 December 2025
Revised: 18 February 2026
Accepted: 24 February 2026
Published: 4 March 2026

building envelope, for example through functional coatings or conductive layers embedded in walls, partitions, or ceilings.

A wide range of EMI shielding materials has been explored, including metallic components, ferrite-based systems, rare-earth-containing absorbers, and lightweight carbon-based materials such as biochars and carbon scaffolds [5,6]. In buildings, conventional solutions often rely on metallic sheets mechanically attached to the envelope; despite their high shielding effectiveness, they are penalized by weight, corrosion susceptibility, limited conformability to complex geometries, and reduced compatibility with standard construction practices [7]. To overcome these drawbacks, cement-based materials have been rendered electromagnetically functional by incorporating conductive carbonaceous phases such as coke powder, short carbon fibres, carbon nanotubes, and graphene-based fillers [8–14]. In parallel, epoxy composites filled with multi-walled carbon nanotubes have demonstrated remarkable absorption in the 3–18 GHz range, further supporting the effectiveness of carbon nanostructures as functional fillers for electromagnetic attenuation [15].

Among carbon-based candidates compatible with large-area building applications, biochar has emerged as a promising and cost-effective option. Biochar is a carbon-rich material obtained by pyrolysis of biomass residues under limited oxygen supply, with established applications in agriculture, soil improvement, water-retention enhancement, and environmental remediation [16–19].

Because biochar can be obtained from a broad range of biomasses, its intrinsic electrical conductivity and dielectric properties can vary significantly depending on feedstock and pyrolysis conditions [5,20,21]. Accordingly, several studies have systematically characterized biochars over different frequency regimes, spanning low-frequency electrical response [20,22] and extending to terahertz-range electromagnetic characterization of biochar-based materials [23]. This evidence has supported the increasing use of biochar as a functional filler in cementitious composites, where both mechanical performance [24–26] and EMI shielding/attenuation properties have been investigated [27].

In particular, cementitious composites filled with commercial wood-based biochar reported shielding effectiveness values up to about 15 dB at 10 GHz (X-band) for 18 wt% biochar, while maintaining good filler dispersion [28]. Further work showed that biochar type and water content, controlled by curing and ageing, can strongly affect performance, with values above 20 dB in the X-band and decreases after prolonged ageing due to loss of physically adsorbed water [29]. Hybrid cement-based mixtures combining biochar with recycled polyvinyl chloride (PVC) also reached shielding effectiveness values of the order of 16 dB in the C-band for appropriate formulations [30]. Biochar typically exhibits intrinsic electrical conductivity in the 0.1–0.2 S/m range, enabling the functionalization of otherwise insulating building materials [31].

Biochar-based coatings have also been applied to common building components such as drywall panels. Measurements between 1 and 18 GHz at different incidence angles indicated that biochar-coated systems can achieve shielding effectiveness comparable to other carbon-based solutions while remaining inexpensive and easy to implement in construction practice [32]. From a sustainability and scalability standpoint, biochar provides a route to carbon-based EMI shielding using low-cost feedstocks and valorizing biomass residues through oxygen-limited thermal conversion. Coupling biochar coatings with widely available gypsum drywall supports large-area deployment with minimal modifications to standard building components.

Shielding behavior is governed by the interplay of absorption, reflection, and multiple-reflection mechanisms, which depend on both material properties and structural design [33]. For layered assemblies, alternating conductive and dielectric layers can enhance multiple-reflection contributions. For instance, Song et al. [34] investigated ∼2 mm-thick sandwich structures with alternating graphene-based conductive films and dielectric spacers, showing that increasing the number of conductive layers can markedly improve shielding effectiveness, partly due to stronger multiple-reflection effects.

Based on this background, the present work investigates biochar-coated drywall panels as a lightweight and construction-friendly solution for electromagnetic shielding in the K-band (18–27 GHz). In this frequency range, electromagnetic compatibility and shielding are of practical interest for several application domains, including high-data-rate satellite communications (e.g., space-to-Earth downlinks commonly allocated around 17.7–20.2 GHz), automotive radar (24 GHz bands), and 5G FR2 millimetre-wave links. Accordingly, reliable shielding performance in the K-band can help mitigate interference in dense electromagnetic environments and in the proximity of sensitive receivers. Biochar-based coatings are integrated within standard multilayer gypsum-board systems [32] to combine the architectural and fire-resistance advantages of drywall with the functional response of a carbonaceous shielding layer. The paper is organized as follows: Section 2 describes the materials and methods; Section 3 presents the experimental results; Section 4 discusses the results and underlying shielding properties; finally, Section 5 summarizes the main conclusions.

2. Materials and Methods

2.1. Preparation of Biochar Paste and Samples

Biochar powder from wood feedstock was purchased by Carlo Erba Reagents S.r.l. (Milan, Italy). The powder was packaged in a closed alumina crucible filled to the top and thermally treated in an oven at 750 °C for 4 h prior to use. Ethyl Hydroxyethyl Cellulose (EHEC) was supplied by SE Tylose GmbH & Co. KG (Wiesbaden, Germany). Ammonia solution 25% w/w was purchased by Sigma-Aldrich S.r.l. (Milan, Italy). The paste was prepared manually by mixing biochar with water (ratio biochar/water = 0.16). Then EHEC and NH_3 were added in the following proportion: 7 g of EHEC to 30 drops of ammonia solution. The mixture was stirred until it became homogeneous and viscous. The paste was spread on a commercial gypsum-drywall panel and allowed to dry at room temperature. Several layers of biochar were applied in order to obtain the densities required for the experimental tests, as shown in Table 1, with a biochar thickness varying between 1.5 and 3 mm.

The drywall panels used are normally available on the market. These are standard panels measuring 1200 × 2000 × 10 mm. To facilitate laboratory operations and SE measurements in the anechoic chamber, the panels were cut into tiles measuring 300 × 300 mm (see Figure 1).

SE measurements were carried out for two configurations: (i) a single drywall panel coated with a biochar paste (D–B) and (ii) a double-panel configuration obtained by stacking two coated panels, resulting in a drywall–biochar–drywall–biochar sandwich (D–B–D–B) (see Figure 1). Multiple biochar layers were applied to each sample to achieve the target surface densities required for the experimental tests (Table 1). Three samples were prepared for each biochar concentration.

Table 1. List of samples and amount of biochar applied.

Sample	Biochar (g/cm^2)	Biochar (Total g per Tile)
reference	-	-
6a, 6b, 6c	0.06	54
9a, 9b, 9c	0.09	81
20a, 20b, 20c	0.20	180

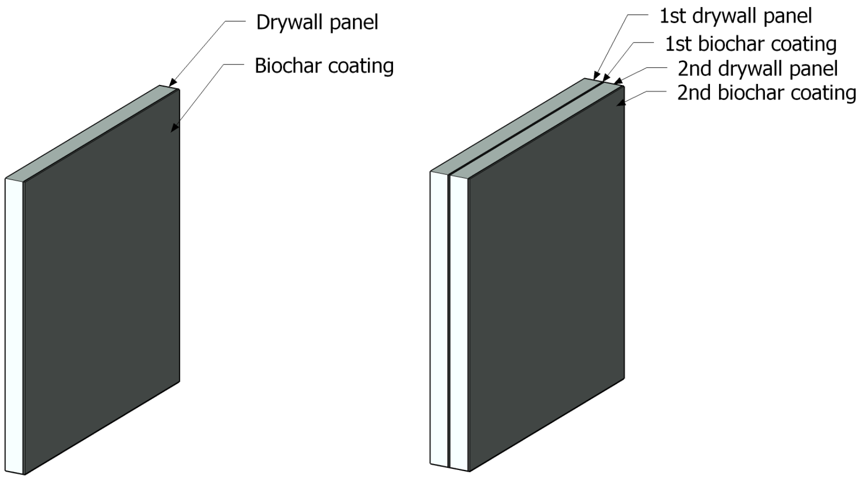

Figure 1. Diagram showing a single panel D-B (**left**) and a double panel D-B-D-B (**right**).

2.2. X-Rays Diffraction (XRD)

X-ray diffraction (XRD) analysis was carried out on a powder diffractometer (Bruker D8 Advance, Bruker Italia S.r.l., Milan, Italy). Diffraction measurements were carried out using a diffractometer equipped with a Cu X-ray tube operating at 40 kV and 40 mA and a Lynxeye XE-T® solid-state detector (Bruker Italia S.r.l., Milan, Italy). The 2θ scanning range was 5–70° with a step size of 0.01° and a total time/step of 19 s. For the identification of the phases, the patterns were analyzed using DIFFRACPLUS EVA© version 5.1.0.5 software and the ICDD-PDF (International Centre for Diffraction Data—Powder Diffraction Files) database (version 2024). The crystallinity index for the biochar was determined by calculating the ratio of the areas corresponding to the crystal and amorphous regions of the X-ray diffractogram.

2.3. Complex Permittivity Measurement Setup

The complex permittivity of the biochar powder and EHEC was measured using a commercial open-ended coaxial sensor specifically suited for liquid and powder (Agilent 85070D, Keysight Technologies, Santa Rosa, CA, USA) and a Network Analyzer (Keysight Technologies, Santa Rosa, CA, USA) [15,35]. The measurement setup is shown in Figure 2. A standard calibration short/air/water was performed before the measurements.

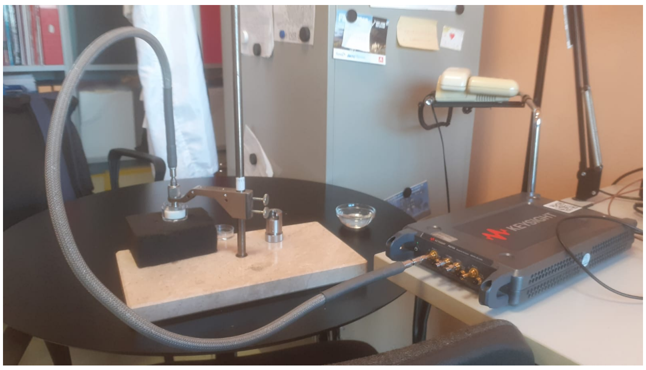

Figure 2. Experimental setup for the measurements of biochar and EHEC powder.

2.4. Multilayered Panel Analysis

The shielding properties of a multilayered structure (see Figure 3) were analyzed using a standard transmission line approach, and by modeling each transmission line of length d1 (d2) with a 2-port transmission matrix, the reflection and transmission coefficient of the entire structure can be obtained [36].

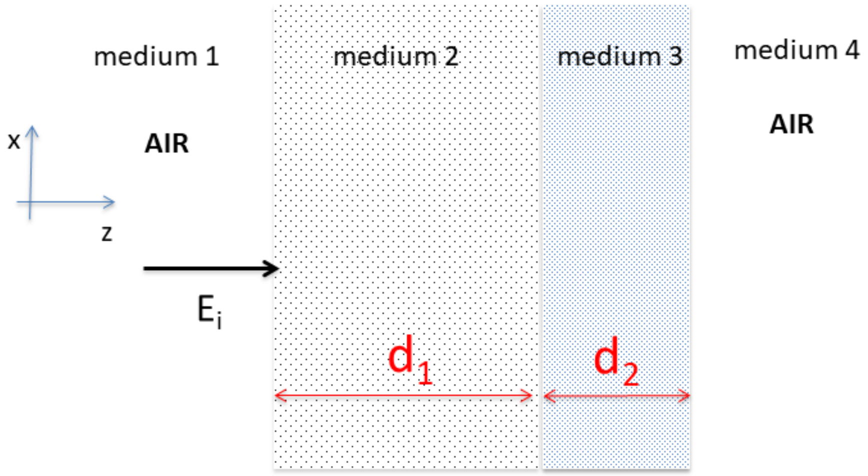

Figure 3. An example of a two-layer structure.

2.5. Transmission Measurement Setup

Transmission measurements were performed in an anechoic chamber (dimensions of 2 × 4 × 2 m). The anechoic chamber has walls, ceiling, and floor covered with pyramidal microwave absorbers designed from 1200 MHz to 90 GHz.

The samples were mounted on a holder made of polymethacrylimide (PMI) foam. The holder was placed between the transmitting and receiving antennas (see Figure 4). Both antennas were horn antennas (18–27 GHz) mounted on a 3-axis positioner and connected to a vector network analyzer (Keysight N5227A) with a time-domain option. Unwanted reflections were removed by transforming frequency domain data into the time domain, applying a gate of 1 ns and then converting back.

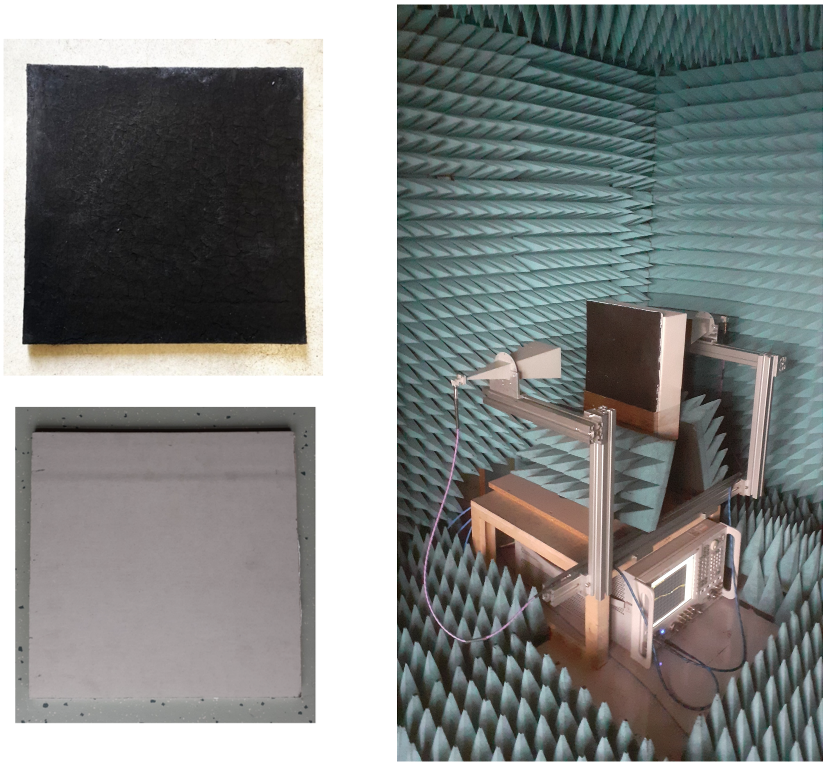

Figure 4. Standard drywall panel (**bottom left**); drywall panel with biochar coating (**top left**); SE measurement setup (**right**).

3. Results

3.1. X-Ray Diffraction (XRD)

XRD analysis was performed to identify the phase composition of the biochar and to evaluate its crystallinity. XRD is a bulk technique, it can identify crystalline phases at 1% mass fraction. XRD analysis revealed the presence of calcite ($CaCO_3$), quartz SiO_2, and traces of lime CaO. The latter is the product of the decomposition of a small amount of calcite during the thermal treatment at 750 °C for four hours. As shown in Figure 5, the powder is rather amorphous, with 65 wt% of amorphous fraction (mainly graphitic carbon). At the top of Figure 5 is shown the diffractogram of the biochar-containing layer: in addition to the peaks of biochar, a broad shoulder is present due to the bump around 20.5° of EHEC.

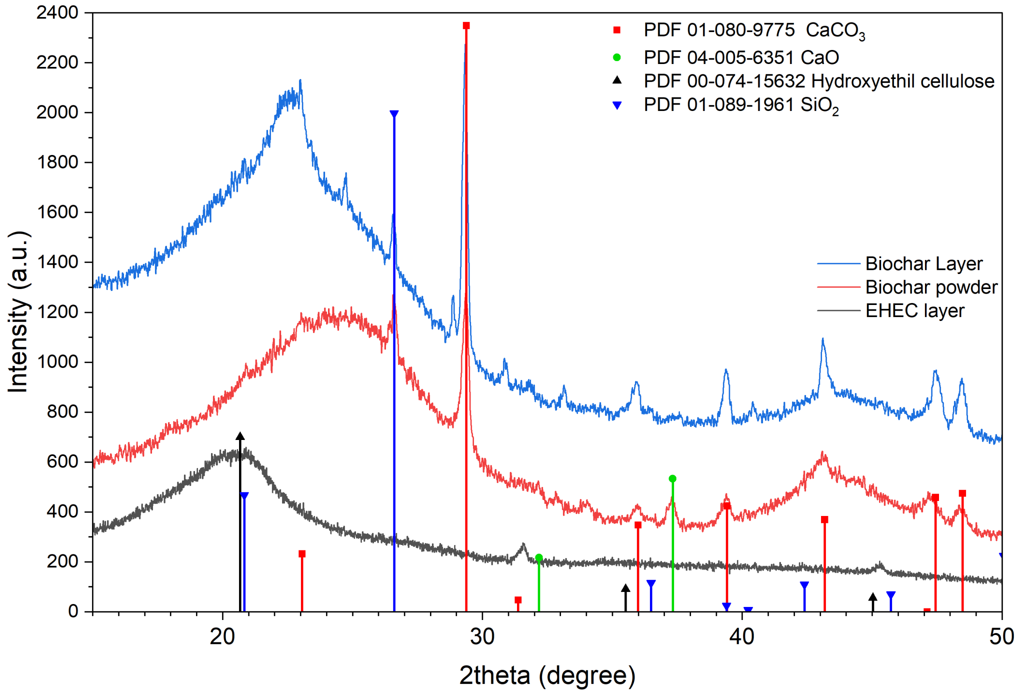

Figure 5. XRD pattern of EHEC, biochar powder, and biochar-containing layer. The main crystalline phases are as follows: in the biochar powder, calcite $CaCO_3$ (PDF 01-080-9775), quartz SiO_2 (PDF 01-089-1961), and lime CaO (PDF 04-005-6351); in the EHEC powder, hydroxyethyl cellulose (PDF 00-074-15632).

3.2. Complex Permittivity Measurements

The components of the coating are biochar powder, water, EHEC powder, and some drops of NH_3. Since water evaporates during the process, measurements of the complex permittivity were performed on the powder of biochar and EHEC. The complex permittivity measured on the individual components can provide guidance in determining the values of SE due to the presence of the coating. The values measured at 18 GHz are shown in Table 2.

The EHEC powder exhibits a relative permittivity of about 1.5 and a low loss tangent ($\tan\delta \approx 0.04$), values that are comparable to those typically reported for gypsum-based materials. As a consequence, EHEC is expected to have a limited impact on the SE of the coating and mainly acts as a rheology modifier and binder for the biochar particles.

However, the biochar powder shows a significantly higher real part of the permittivity (around 10) and a relatively large loss tangent ($\tan\delta \approx 0.5$). These characteristics indicate that the biochar phase is expected to play a dominant role in determining the shielding effectiveness of the coated panels.

https://doi.org/10.3390/electronics15051073

These measured values of the complex permittivity were used as an initial guess to fit the measurements with the transmission lines model.

Table 2. Measured complex permittivity of biochar and EHEC powder at 18 GHz.

Powder	Real Part	tan δ
biochar	10	0.5
EHEC	1.5	0.04

3.3. Analytical Model Results

The bare drywall panel and the biochar-coated drywall were analyzed using the analytical model described in Section 2.4. For the uncoated panel, the best agreement with the experimental data was obtained by assuming an effective thickness of 9.1 mm. For the coated specimens, the biochar-layer thickness was treated as a fitting parameter: the best fit was achieved with a 2.0 mm layer for the 0.09 g/cm^2 coating and with a 3.8 mm layer for the 0.2 g/cm^2 coating. The corresponding model–measurement comparison is reported in Figure 6.

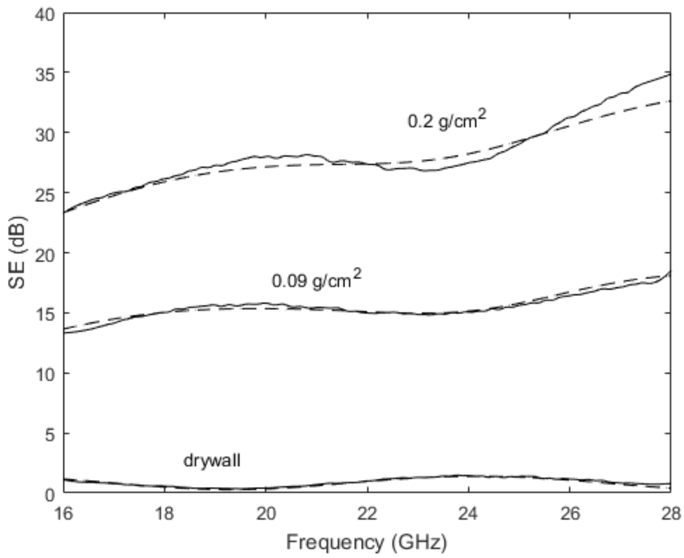

Figure 6. Comparison between model (dashed line) and measurements (solid line) for the drywall panel and the drywall panel with 0.09 g/cm^2 and 0.20 g/cm^2 of biochar.

3.4. SE Measurements

In this section, the SE measured on single panels and double panels with biochar coating with different density are shown and compared with the reference sample.

As a general guideline, shielding materials with a shielding effectiveness (SE) below 10 dB are regarded as materials with poor protection. Values between 10 and 30 dB indicate limited shielding performance, while SE values exceeding 30 dB are typically considered adequate for most commercial and industrial uses [37].

For single panels, if we consider a biochar density of 0.06 g/cm^2, the shielding effectiveness is at least 10 dB (Figure 7 left). The consistency between the three samples of a set is high, with a maximum deviation of less than 1 dB between the different panels. In the case of a biochar density of 0.09 g/cm^2, the shielding effectiveness is at least 14 dB. Regarding the dispersion, reproducibility is excellent: the curves corresponding to the three samples are almost superimposed. In the case of drywall panels with a biochar density of 0.20 g/cm^2, SE values exceed 23 dB. There is a greater dispersion in this case, probably due to fabrication defects that affect the uniformity of the coating at higher densities.

In the case of double panels, the SE of the reference sample (two panels of drywall without biochar with total thickness 20 mm) is almost 0 dB throughout the whole frequency range. If we consider double panels with a biochar density of 0.06 g/cm^2, the SE value is at least 17 dB. In the case of double panels with a biochar density of 0.09 g/cm^2 the SE is at least 23 dB, reaching peaks up to 35 dB depending on the frequency. In this case, we note a greater dispersion of the measured values of the three samples. This is probably due to some defects in the deposition process or non-uniform coupling between the panels. Finally, in the case of double panels with a biochar density of 0.20 g/cm^2, the SE is at least 46 dB. These samples show the highest performance, reaching an average SE value around 50 dB.

This behavior is consistent with the complex permittivity measurements, which showed that the EHEC powder has dielectric properties similar to those of the gypsum board, whereas the biochar exhibits a much higher real permittivity (around 10) and loss tangent ($\tan\delta \approx 0.5$) and therefore is expected to play a dominant role in the shielding effectiveness of the coated panels and to increase the SE with increase of the density (see Table 3).

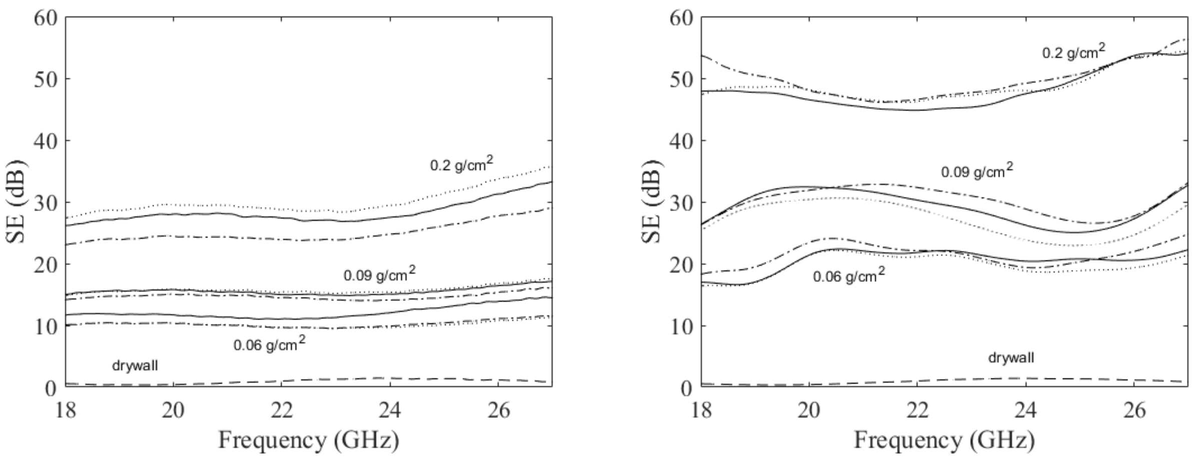

Figure 7. SE measurements with biochar 0.06, 0.09, and 0.20 g/cm^2 for single panel (**left**) and double panel (**right**) configuration. On the bottom is reported the SE of the reference sample without biochar marked as drywall.

Table 3. Minimum value of SE for the various configurations.

Sample	Biochar 0 g/cm^2	Biochar 0.06 g/cm^2	Biochar 0.09 g/cm^2	Biochar 0.20 g/cm^2
ref. (single or double)	0.5 dB	–	–	–
single panel	–	10 dB	14 dB	23 dB
double panel	–	17 dB	23 dB	46 dB

4. Discussion

Based on the data collected so far, we correlated the biochar density with the SE for the extremes of the range and for the central frequency (18, 22, and 27 GHz). Results are shown in Figure 8 left in the case of single panel and in Figure 8 right for double panels.

The comparative analysis of the single panel and double panel charts reveals that both configurations follow a power law $y = Ax^B$ (see Table 4). In the case of the single panel, the multiplier (A) increases strictly with frequency (74.60 at 18 GHz to 106.93 at 27 GHz). In the double panel, these coefficients effectively double, peaking at 195.39. In both the single and double panel configurations, SE increases with increasing biochar density and shows a slight upward trend with frequency.

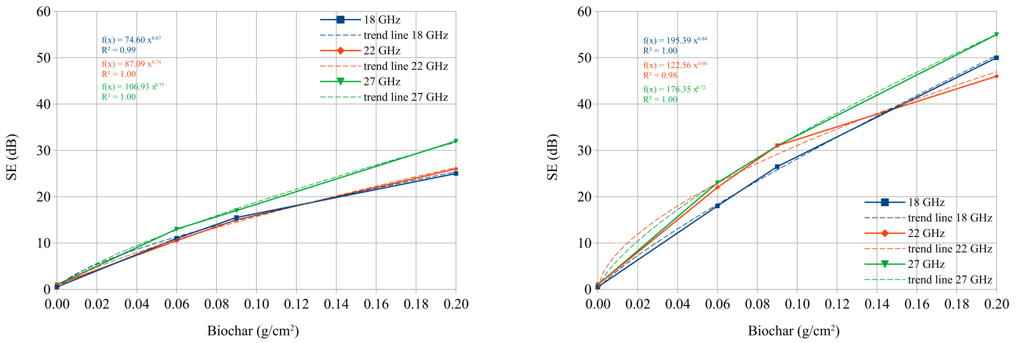

Figure 8. SE measurements of single (**left**) and double (**right**) panels with biochar at 0.06 g/cm^2, 0.09 g/cm^2, 0.20 g/cm^2 and fixed frequency of 18 GHz, 22 GHz and 27 GHz.

Table 4. Trend line equations and correlation coefficients (R^2) for Single and Double panel configurations at different frequencies.

Frequency (GHz)	Trend Line Equation	R^2 Value
	Single Panel Configuration	
18	$f(x) = 74.60\,x^{0.67}$	0.99
22	$f(x) = 87.09\,x^{0.74}$	1.00
27	$f(x) = 106.93\,x^{0.75}$	1.00
	Double Panel Configuration	
18	$f(x) = 195.39\,x^{0.84}$	1.00
22	$f(x) = 122.56\,x^{0.60}$	0.98
27	$f(x) = 176.35\,x^{0.72}$	1.00

To evaluate the improvement provided by the double-layer configuration across the entire frequency band (18–27 GHz), we introduced the Gain Coefficient (K_g), defined as

$$K_g = \frac{SE_{double}}{SE_{single}} \tag{1}$$

Instead of relying on single frequency points, which may be subject to local resonances, we analyzed the statistical behavior of K_g over the entire considered bandwidth. Table 5 summarizes the performance in terms of average gain ($K_{g,avg}$) and the minimum guaranteed threshold ($K_{g,min}$).

Table 5. Summary of the Gain Coefficient (K_g) analysis: average values and minimum guaranteed thresholds over the 18–27 GHz band.

Biochar Density (g/cm^2)	Average Gain ($K_{g,avg}$)	Minimum Threshold ($K_{g,min}$)
0.06	1.95	$>$1.60
0.09	1.90	$>$1.70
0.20	1.70	$>$1.55

The experimental data reveal that the Average Gain Coefficient remains high across all densities, ranging from 1.70 to 1.95. For lower densities (0.06 and 0.09 g/cm^2), the value is remarkably close to the theoretical factor of 2 (linear doubling in dB). As the density increases to 0.20 g/cm^2, the observed value settles slightly lower ($K_g \approx 1.7$). This deviation is physically attributed to the multiple reflections occurring at the interface between the two panels and potential saturation effects at high attenuation levels, which introduce interference mechanisms that slightly reduce the cumulative efficiency compared to a perfectly additive absorption model.

From an engineering perspective, the "worst-case" performance is often more critical than the average. By analyzing the frequency-by-frequency ratio between the double and single configurations, we established a minimum efficiency threshold ($K_{g,min}$) for each density:

- The 0.06 g/cm^2 samples ensure a gain factor consistently above 1.60 across the band.
- The 0.09 g/cm^2 samples demonstrate robust stability, maintaining a gain threshold of at least 1.70.
- The 0.20 g/cm^2 samples, despite the higher absolute shielding values, guarantee a gain factor greater than 1.55.

This confirms that the double-layer configuration reliably boosts the shielding performance by a factor of at least 1.55 to 1.70 (depending on density) compared to the single layer, regardless of the operating frequency. Finally, the double-panel configuration with a biochar density of 0.20 g/cm^2 exhibits a remarkably uniform behavior, maintaining an shielding effectiveness of at least 46 dB. This characteristic is particularly advantageous compared to conventional shielding materials, which often rely on resonance mechanisms and thus deliver peak performance only within narrow frequency intervals. In contrast, the proposed biochar-based composite demonstrates robust broadband attenuation, ensuring reliable protection in the K-band.

A comparison with representative shielding solutions used in building applications and with selected microwave/mmWave EMI-shielding approaches is reported in Table 6 to contextualize the measured K-band SE of the proposed panels.

Table 6. Comprehensive summary of shielding and absorbing materials, including recent updates on biochar-based and cement-based composites.

Filler/Material	Thickness	SE	Frequency Range	Ref.
Highly Filled Biochar (80 wt%)/UHMWPE/LLDPE	3 mm	>40 dB	300 MHz–1.5 GHz	[38]
Biochar-Gypsum Composites (Sustainable drywall)	15 mm	5 dB to 15 dB	800 MHz–6 GHz	[39]
Common Building Materials (Brick, Concrete)	300 mm	<11.8 dB	1–9 GHz	[40]
Composites, 15% w/w multi-walled carbon nanotube/cement	2 mm	<28 dB	8.2–12.4 GHz	[11]
Single panel (0.2 g/cm^2)	9.5 mm + 3 mm	>23 dB	18–27 GHz	this work
Double panel (0.2 g/cm^2)	2 × (9.5 + 3) mm	>46 dB	18–27 GHz	this work

Note: SE = Shielding Effectiveness; UHMWPE = Ultra-High Molecular Weight Polyethylene; LLDPE = Linear Low Density Polyethylene.

5. Conclusions

This study evaluated the electromagnetic shielding effectiveness (SE) of drywall panel coating with biochar in the 18–27 GHz range, with particular attention to configurations compatible with standard building practice. By varying the surface density of the biochar coating and combining single- and double-panel assemblies, it was possible to quantify how both material design and architectural assembly contribute to electromagnetic interference mitigation in the K-band.

The main quantitative outcomes can be summarized as follows:

- SE follows a power law defined by $SE = A \cdot x^B$, where x is the biochar surface density. Single-panel configurations exhibited a near-perfect fit ($R^2 \approx 0.99$), ensuring high predictability of performance as a function of coating density.
- For single panels, the coefficient A increases steadily with frequency, rising from 74.60 at 18 GHz to 106.93 at 27 GHz. This indicates that biochar coatings become progressively more effective at higher frequencies within the K-band.
- In the double-panel configuration, the shielding effectiveness significantly improves, showing an average gain coefficient ($K_{g,avg}$) ranging from 1.70 to 1.95 depending on the density. While a theoretical doubling of the absorber thickness would imply a factor of 2, the observed values are slightly lower due to multiple internal reflections at the panel interface. Nevertheless, the analysis confirms a guaranteed minimum gain threshold ($K_{g,min}$) between 1.55 and 1.70 across the entire band, ensuring consistent performance enhancement regardless of frequency fluctuations.
- Across the 18–27 GHz band, panels with a biochar density of 0.20 g/cm^2 demonstrate superior performance, yielding a SE of at least 23 dB for single panels and being greater than 46 dB for double panels. This high attenuation is remarkably uniform across the investigated spectrum, providing reliable broadband protection rather than the narrow-band peaks typical of resonant shielding materials.

From a broader perspective, these results demonstrate that relatively thin biochar coatings, applied onto standard gypsum boards, can provide a meaningful level of electromagnetic shielding without altering the overall geometry or installation procedures of drywall systems. The consistent gain in dB when passing from single to double panels suggests that shielding performance can be tailored by combining architectural solutions with appropriate biochar dosage. In this way, designers are offered an additional degree of freedom in controlling indoor exposure to high-frequency fields.

In addition, the use of biochar aligns with current sustainability targets in the construction sector. Biochar can be produced from biomass residues and waste streams, and gypsum boards themselves already incorporate recycled components, making the proposed system intrinsically compatible with circular-economy approaches. The combination of electromagnetic functionality and resource-efficient materials therefore opens the way to building products that simultaneously address both technological and environmental requirements.

The integration of biochar into drywall systems thus emerges as a sustainable and high-performance solution for EMI shielding in modern telecommunication environments, offering a practical route to functional building envelopes that can be tuned to specific shielding requirements without departing from conventional construction practice.

Author Contributions: Conceptualization, G.R., P.S. and I.N.S.; Methodology, G.R., P.S., I.N.S. and M.P.; Software, G.R., P.S. and I.N.S.; Validation, G.R., P.S., I.N.S. and M.P.; Formal analysis, G.R., P.S. and I.N.S.; Investigation, G.R., P.S., I.N.S. and M.P.; Data curation, G.R., P.S. and I.N.S.; Writing—original draft preparation, G.R., P.S. and I.N.S.; Writing—review & editing, G.R., P.S., I.N.S. and M.P.; Visualization, G.R., P.S. and I.N.S.; Supervision, G.R., P.S. and I.N.S.; Project administration, G.R., P.S. and I.N.S. All authors have read and agreed to the published version of the manuscript.

Funding: This research received no external funding.

Data Availability Statement: Data will be made available upon request.

Acknowledgments: The authors would like to thank Zahra Alinaghi and Davide di Summa for preparing the samples, Gianluca Dassano for his assistance in performing the shielding effectiveness measurements, and Laura De Martin for the help with the pictures.

Conflicts of Interest: The authors declare no conflicts of interest.

References

1. Huamin, J.; Zhao, Z.; Zeng, Y.; Chang, Y.; Fan, F.; Wang, C.; See, K. A review of intentional electromagnetic interference in power electronics: Conducted and radiated susceptibility. *IET Power Electron.* **2024**, *17*, 1487–1506. [CrossRef]
2. Fan, F.; Zhao, Z.; Jie, H.; See, K.Y. Systematic testing, simulation, and mitigation of IEMI risks in medium-voltage substations. *Measurement* **2024**, *228*, 114334. [CrossRef]
3. Banik, S.; Bandyopadhyay, S.; Ganguly, S. Bioeffects of microwave—A brief review. *Bioresour. Technol.* **2003**, *87*, 155–159. [CrossRef]
4. Kim, J.H.; Lee, J.K.; Kim, H.G.; Kim, K.B.; Kim, H.R. Possible effects of radiofrequency electromagnetic field exposure on central nerve system. *Biomol. Ther.* **2019**, *27*, 265. [CrossRef] [PubMed]
5. Marinković, D.; Dorontić, S.; Kepić, D.; Haddadi, K.; Yasir, M.; Nardin, B.; Jovanović, S. New Electromagnetic Interference Shielding Materials: Biochars, Scaffolds, Rare Earth, and Ferrite-Based Materials. *Nanomaterials* **2025**, *15*, 541. [CrossRef]
6. Demirtaş, H.; Dayı, M. A Proposal for Electromagnetic Performance in Cementitious Systems: Carbon Fiber and Copper Slag. *Buildings* **2025**, *15*, 3634. [CrossRef]
7. Kwon, J.H.; Hyoung, C.H.; Park, H.H. Analysis of Shielding Performance in Double-Layered Enclosures with Integrated Absorbers. *Electronics* **2024**, *13*, 4345. [CrossRef]
8. Cao, J.; Chung, D.D.L. Coke powder as an admixture in cement for electromagnetic interference shielding. *Carbon* **2003**, *41*, 2433–2436. [CrossRef]
9. Muthusamy, S.; Chung, D. Carbon-Fiber Cement-Based Materials for Electromagnetic Shielding. *ACI Mater. J.* **2010**, *107*, 602–610. [CrossRef]
10. Li, K.; Wang, C.; Li, H.; Li, X.; Ouyang, H.; Wei, J. Effect of chemical vapor deposition treatment of carbon fibers on the reflectivity of carbon fiber-reinforced cement-based composites. *Compos. Sci. Technol.* **2008**, *68*, 1105–1114. [CrossRef]
11. Singh, A.P.; Gupta, B.K.; Mishra, M.; Govind; Chandra, A.; Mathur, R.; Dhawan, S. Multiwalled carbon nanotube/cement composites with exceptional electromagnetic interference shielding properties. *Carbon* **2013**, *56*, 86–96. [CrossRef]
12. Liu, Z.; Ge, H.; Wu, J.; Chen, J. Enhanced electromagnetic interference shielding of carbon fiber/cement composites by adding ferroferric oxide nanoparticles. *Constr. Build. Mater.* **2017**, *151*, 575–581. [CrossRef]
13. Chen, J.; Zhao, D.; Ge, H.; Wang, J. Graphene oxide-deposited carbon fiber/cement composites for electromagnetic interference shielding application. *Constr. Build. Mater.* **2015**, *84*, 66–72. [CrossRef]
14. Mazzoli, A.; Corinaldesi, V.; Donnini, J.; Di Perna, C.; Micheli, D.; Vricella, A.; Pastore, R.; Bastianelli, L.; Moglie, F.; Mariani Primiani, V. Effect of graphene oxide and metallic fibers on the electromagnetic shielding effect of engineered cementitious composites. *J. Build. Eng.* **2018**, *18*, 33–39. [CrossRef]
15. Giorcelli, M.; Savi, P.; Delogu, A.; Miscuglio, M.; Yahya, Y.M.H.; Tagliaferro, A. Microwave absorption properties in epoxy resin Multi Walled Carbon Nanotubes composites. In Proceedings of the 2013 International Conference on Electromagnetics in Advanced Applications (ICEAA), Torino, Italy, 9–13 September 2013; pp. 1139–1141. [CrossRef]
16. Ahmad, M.; Rajapaksha, A.U.; Lim, J.E.; Zhang, M.; Bolan, N.; Mohan, D.; Vithanage, M.; Lee, S.S.; Ok, Y.S. Biochar as a sorbent for contaminant management in soil and water: A review. *Chemosphere* **2014**, *99*, 19–33. [CrossRef]
17. Amin, F.R.; Huang, Y.; He, Y.; Zhang, R.; Liu, G.; Chen, C. Biochar applications and modern techniques for characterization. *Clean Technol. Environ. Policy* **2016**, *18*, 1457–1473. [CrossRef]
18. Tan, X.; Liu, Y.; Zeng, G.; Wang, X.; Hu, X.; Gu, Y.; Yang, Z. Application of biochar for the removal of pollutants from aqueous solutions. *Chemosphere* **2015**, *125*, 70–85. [CrossRef] [PubMed]
19. Maroušek, J.; Vochozka, M.; Plachỳ, J.; Žák, J. Glory and misery of biochar. *Clean Technol. Environ. Policy* **2017**, *19*, 311–317. [CrossRef]
20. Yao, H.; Xiong, Y.; Pickles, C.; Hutcheon, R.; Pahnila, M.; Hagström, A.; Fabritius, T.; Omran, M. Dielectric properties of biomass by-products generated from wood and agricultural industries in Finland. *Bioresour. Technol.* **2025**, *426*, 132319. [CrossRef]
21. Gioti, C.; Vasilopoulos, K.C.; Baikousi, M.; Salmas, C.E.; Ntaflos, A.; Paipetis, A.S.; Viskadourakis, Z.; Ikram, R.; Agathopoulos, S.; Kenanakis, G.; et al. Enhanced Gypsum Boards with Activated Carbon Composites and Phase Change Materials for Advanced Thermal Energy Storage and Electromagnetic Interference Shielding Properties. *Micro* **2024**, *4*, 61–79. [CrossRef]
22. Nikolopoulos, C.D.; Baklezos, A.T.; Kapetanakis, T.N.; Vardiambasis, I.O.; Tsubota, T.; Kalderis, D. Characterization of the Electromagnetic Shielding Effectiveness of Biochar-Based Materials. *IEEE Access* **2023**, *11*, 6413–6420. [CrossRef]
23. Park, W.; Kim, H.; Park, H.; Choi, S.; Hong, S.J.; Bahk, Y.M. Biochar as a low-cost, eco-friendly, and electrically conductive material for terahertz applications. *Sci. Rep.* **2021**, *11*, 18498. [CrossRef]
24. Alireza Jafari, P.S. Biochar and recycled gypsum drywall in concrete: Role and effects on compressive behavior, microstructure, and carbon footprint. *J. Sustain.-Cem.-Based Mater.* **2025**, *14*, 119–144. [CrossRef]
25. Tayyab, S.; Ferdous, W.; Lokuge, W.; Siddique, R.; Manalo, A. Biochar in cementitious composites: A comprehensive review of properties, compatibility, and prospect of use in sustainable geopolymer concrete. *Resour. Conserv. Recycl. Adv.* **2025**, *25*, 200242. [CrossRef]

26. Zhao, Z.; El-Naggar, A.; Kau, J.; Olson, C.; Tomlinson, D.; Chang, S.X. Biochar affects compressive strength of Portland cement composites: A meta-analysis. *Biochar* **2024**, *6*, 21. [CrossRef] [PubMed]
27. Gupta, S.; Tai, N.H. Carbon materials and their composites for electromagnetic interference shielding effectiveness in X-band. *Carbon* **2019**, *152*, 159–187. [CrossRef]
28. Yasir, M.; di Summa, D.; Ruscica, G.; Natali Sora, I.; Savi, P. Shielding properties of cement composites filled with commercial biochar. *Electronics* **2020**, *9*, 819. [CrossRef]
29. Di Summa, D.; Ruscica, G.; Savi, P.; Pelosato, R.; Natali Sora, I. Biochar-containing construction materials for electromagnetic shielding in the microwave frequency region: The importance of water content. *Clean Technol. Environ. Policy* **2023**, *25*, 1099–1108. [CrossRef]
30. Ruscica, G.; Peinetti, F.; Natali Sora, I.; Savi, P. Analysis of Electromagnetic Shielding Properties of Cement-Based Composites with Biochar and PVC as Fillers. *C* **2024**, *10*, 21. [CrossRef]
31. Geetha, S.; Satheesh Kumar, K.; Rao, C.R.; Vijayan, M.; Trivedi, D. EMI shielding: Methods and materials—A review. *J. Appl. Polym. Sci.* **2009**, *112*, 2073–2086. [CrossRef]
32. Savi, P.; Ruscica, G.; di Summa, D.; Natali Sora, I. Shielding Effectiveness Measurements of Drywall Panel Coated with Biochar Layers. *Electronics* **2022**, *11*, 2312. [CrossRef]
33. Celozzi, S.; Araneo, R.; Burghignoli, P.; Lovat, G. *Electromagnetic Shielding: Theory and Applications*; John Wiley & Sons: Hoboken, NJ, USA, 2022.
34. Song, W.L.; Gong, C.; Li, H.; Cheng, X.D.; Chen, M.; Yuan, X.; Chen, H.; Yang, Y.; Fang, D. Graphene-based sandwich structures for frequency selectable electromagnetic shielding. *ACS Appl. Mater. Interfaces* **2017**, *9*, 36119–36129. [CrossRef]
35. Giorcelli, M.; Savi, P.; Yasir, M.; Miscuglio, M.; Yahya, M.H.; Tagliaferro, A. Investigation of epoxy resin/multiwalled carbon nanotube nanocomposite behavior at low frequency. *J. Mater. Res.* **2015**, *30*, 101–107. [CrossRef]
36. Pozar, D.M. *Microwave Engineering: Theory and Techniques*; John Wiley & Sons: Hoboken, NJ, USA, 2021.
37. Sankaran, S.; Deshmukh, K.; Ahamed, M.B.; Khadheer Pasha, S. Recent advances in electromagnetic interference shielding properties of metal and carbon filler reinforced flexible polymer composites: A review. *Compos. Part A Appl. Sci. Manuf.* **2018**, *114*, 49–71. [CrossRef]
38. Li, S.; Huang, A.; Chen, Y.J.; Li, D.; Turng, L.S. Highly filled biochar/ultra-high molecular weight polyethylene/linear low density polyethylene composites for high-performance electromagnetic interference shielding. *Compos. Part B Eng.* **2018**, *153*, 277–284. [CrossRef]
39. Natalio, F.; Corrales, T.P.; Feldman, Y.; Lew, B.; Graber, E.R. Sustainable lightweight biochar-based composites with electromagnetic shielding properties. *ACS Omega* **2020**, *5*, 32490–32497. [CrossRef] [PubMed]
40. Pavlík, M.; Bereš, M.; Beňa, L'. The Influence of Various Commonly Used Building Materials on the Shielding Effectiveness, Reflection and Absorption of the Electromagnetic Wave. *Appl. Sci.* **2024**, *14*, 2521. [CrossRef]